RGNZ/MGPB

Comparison of The Erosion Prediction Models from USLE, MUSLE and RUSLE in the Poleang River Basin

Rudarsko-geološko-naftni zbornik
(The Mining-Geology-Petroleum Engineering Bulletin)
DOI: 10.17794/rgn.2026.5.13

Original scientific paper

Septianto Aldiansyah[1]*, Amniar Ati[1], Fitriyani Saudi[1], Andrias Andrias[1]
[1] *Faculty of Teacher Training and Education, Halu Oleo University, Kendari, 93232, Indonesia.*

Abstract
Water erosion is a serious global problem due to land degradation, including in Indonesia. This phenomenon has been exacerbated by climate change and anthropogenic interventions into the natural environment in recent decades. Although empirical modelling is a viable approach for predicting soil degradation, its implementation across extensive, ungauged areas is often hindered by data scarcity and inconsistency. This research evaluates and contrasts the efficiency of three USLE-based frameworks in quantifying water-induced erosion within the Poleang River Basin. The specific erosion estimates obtained across the Poleang River Basin surface are 252 t/ha^{-1}/year^{-1}, 210 t/ha^{-1}/year^{-1}, and 230 t/ha^{-1}/year^{-1}, respectively. These three models produced relatively similar estimates, with R^2 values ranging from 91% to 99%. Notably, the USLE model exhibited a broader spatial heterogeneity in risk distribution compared to the MUSLE and RUSLE counterparts. In this context, the canopy cover factor emerged as a more decisive parameter in accounting for elevated erosion rates within the study area.

Keywords:
Geospatial analysis; soil loss estimation; GIS-integrated modelling; USLE-based frameworks; Poleang River Basin

1. Introduction

Soil erosion is a serious and threatening problem for almost all countries in the world. This process has caused significant damage to the physical, chemical, and biological properties of soil (**Lal et al., 2000**). The phenomenon is widely recognized as a diverse and variable landscape occurrence. The release and transport of particles in the soil is mentioned as the most common factor causing this variation in runoff.

Many past studies have observed the effect of climate change on soil erosion rates (**Bryan & Albritton, 1944; Leopold, 1951; Ruhe and Scholtes, 1956**). Factors such as changes in rainfall and runoff (**Bangash et al., 2013; Chiew et al., 1995**), high rainfall intensity (**Tang et al., 2015; Zhang, 2012**), and changes in rainfall distribution patterns (**Maeda et al., 2010**) are direct factors contributing to this phenomenon.

Indonesia, like other tropical countries, is also among the most vulnerable to land degradation. Sustaining land degradation can significantly reduce the long-term productivity of agricultural areas that are already stressed by various human interventions and natural environmental stressors. Given the importance of this issue, resource management for sustainable agriculture is an unavoidable issue.

Soil depletion driven by water is a critical environmental challenge for Indonesia's tropical regions. This problem has significant negative impacts, such as reduced soil productivity. According to **Syaf et al. (2022)**, approximately 20% of the land is seriously critical. Water erosion is also a real threat and a key issue in many river basins in Indonesia (**Ikhwali et al., 2022**). Furthermore, other impacts include waterway pollution, water availability deficits, property damage from runoff with higher soil content, requiring reimbursement, and environmental management. Given the seriousness of this problem, understanding the characteristics of climate, topography, soil properties, vegetation, and land management is crucial because they are considered to control water erosion.

Studies measuring soil erosion by water in the Poleang River Basin are still limited. Based on sediment load calculations, the average indirect erosion rate is estimated at 1.6 t/ha^{-1}/year^{-1} (**Gandri et al., 2023**). Specific erosion tends to vary between regions, with the westernmost to central regions being most affected at 28.69% (**Syaf et al., 2022**). However, previous research has focused solely on evaluating hydrological function (**Gandri et al., 2023**) and assessing land status (**Syaf et al., 2022**). Existing regional soil erosion studies have not yet clarified the driving factors and the relationships with the original

* Corresponding author: Septianto Aldiansyah
e-mail address: septianto.aldiansyah@uho.ac.id
Received: 23 February 2026. Accepted: 9 June 2026.
Available online: 26 October 2026

data sources that influence variations in soil erosion rates. This gap hinders understanding the contribution of each soil type to total soil loss.

Evaluating and detecting eroded areas is a complex task that can be identified by integrating data sources such as spatial data, field measurements, surveys, and satellite imagery using geographic information systems. Different techniques exist for quantifying soil erosion rates and predicting how sediment is transported. Various models were developed by considering physical aspects such as Area Non-point Source Watershed Environment (ASNWERS) (**Beasley et al., 1980**), Annualized Agricultural Non-Point Source Pollutant Loading (AnnANPSPL), Erosion-Productivity Impact Calculator (EPIC) model (**Williams et al., 1985**), Chemicals Runoff and Erosion from Agricultural (CREAMS) model (**Knisel, 1980**), Simulator for Water Resources in Rural Basins (SWRRB) model (**Williams et al., 1985**), the Groundwater Loading Effect of Agricultural Management Systems (GLEAMS) model (**Leonard et al., 1987**), the Water Erosion Prediction Project (WEPP) model (**Nearing et al., 1989**), and the Soil Erosion Model for Mediterranean Areas (SEMMED) model (**Leonard et al., 1987**). The development of such models stems from either practical observations, conceptual frameworks, or a hybrid of both approaches.

Mathematical laws, confirmed by experimental or observational data, form the core of these empirical hydrological models. A common and widely applied model for analyzing the relationship between soil erosion and runoff is the Universal Soil Loss Equation (USLE) (**Wischmeier & Smith, 1978, 1965**). This basic model was later modified into a modified version of the USLE (MUSLE) (**Williams, 1975**) to identify sediment transport by considering runoff volume instead of rainfall erosion power. Through experimental exploration and the abundance of data and resources, the MUSLE model was subsequently further refined by considering soil loss indicators that incorporate the basic provisions of the USLE and correct some inaccuracies in the basic calculations used in determining its factors. This new model is known as the Revised Universal Soil Loss Equation (RUSLE) (**Renard, 1997**).

Statistical models in this context have become a frequently applied method for predicting losses caused by surface erosion. The model can analyze the average annual temporal erosion rate by considering factors considered to influence erosion rates, such as rainfall, topographic soil type, cultivation system, and conservation tillage.

The USLE model was initially used only in agricultural systems, but has since been applied to non-agricultural settings. This model has been successfully adopted at regional and watershed scales (**Bera, 2017; Elaloui et al., 2017**).

The practical application of USLE/RUSLE over expansive areas relies heavily on geospatial tools like GIS and remote sensing, which have been instrumental in advancing soil loss detection and conservation efforts since the late 20th century. Remote sensing and Geographic Information Systems (GIS) have become effective tools for collecting and aggregating spatial information at the landscape scale. This technology allows for the determination of each erosion factor per unit with a more detailed resolution (**Kinnell, 2001**). This technique also allows for open, more concise spatial monitoring and evaluation of soil erosion, resulting in high accuracy even over a large study area.

Many studies have compared erosion estimation models such as USLE, MUSLE, and RUSLE, given their differing approaches to erosivity mechanisms and sensitivity (**Djoukbala et al., 2019; Romdania & Herison, 2024**). Finding an appropriate model is crucial, especially when actual runoff factors influence river erosion and sedimentation rates (**Romdania & Herison, 2024**). For instance, similar multi-model assessments in tropical catchments in Asia and sub-tropical river basins have shown that while USLE and RUSLE provide robust macro-level structural hazard mapping, MUSLE offers superior sensitivity in capturing localized sediment yields driven by high-intensity storm events. Its relevance is further strengthened given the region's hydrometeorological characteristics and the dynamics of land-use change, which cause significant variations in runoff and erosion responses (**Millward & Mersey, 1999; Obaid & Shahid, 2017; Thomas et al., 2018b; Vijith & Dodge-Wan, 2018**). Applying this multi-model comparative approach to the Poleang River Basin is crucial; its sharp topographic gradients and vulnerability to changing hydrological regimes demand a dual evaluation of both climate-driven and runoff-induced erosion processes. Therefore, this study remains necessary to ensure the model's suitability for representing soil erosion processes in the physical and climatic conditions of watersheds in Indonesia.

Based on this description, this research seeks to evaluate soil loss predictions by comparing the original USLE, its modified (MUSLE), and revised (RUSLE) counterparts. This assessment is conducted within the Poleang River Basin, leveraging the synergy between remote sensing and GIS technologies in a region characterized by its comprehensive data accessibility.

2. Methods

2.1. Study Area

The Poleang River Basin drains an area of 111,723.54 ha, with a main river length of 273.35 km and a river width varying between 15 and 30 meters (see **Figure 1; Table 1**). This ecologically important area encompasses the Bombana, Kolaka, and East Kolaka Regencies. It serves as a water catchment and drainage basin, and faces environmental management issues resulting from human activities.

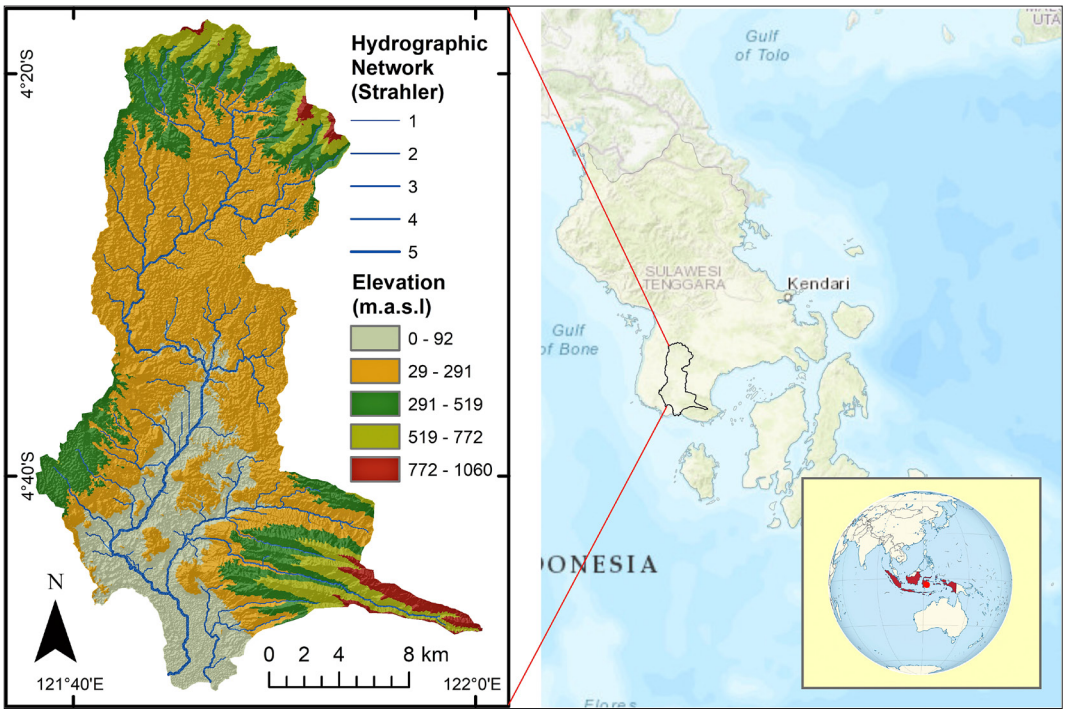


Figure 1: Study Area

Table 1: Morphometric characteristics of the Poleang River Basin

Parameters	Unit	Value
Area A	ha	111,723.54
Perimeter P	km	219.64
Compactness Coefficient IC	-	1,854
Peak elevation H_{max}	m	1,060
Minimum elevation H_{min}	m	0
Average basin height H_{mean}	m	241.73
Elevation to 95% area	m	909
Elevation to 50% area	m	212
Elevation to 5% area	m	10
Longitudinal rectangle dimension L	km	273.35
Lateral rectangle dimension *l*	km	15-30

The Poleang River Basin encompasses a series of mountains and plateaus, particularly in the north and southeast, which also feature peaks with elevations exceeding 1,000 meters. The slope in this region is relatively gentle, reaching 44.90%. The north and southeast represent steep slope zones with slopes >45° (<2%). This watershed is characterized by a dendritic river flow pattern. The upstream area serves as the primary catchment area, while the relatively gentle middle section serves as an intermediary and utilization area. The downstream area comprises an alluvial plain with a higher sediment concentration.

2.2. Data

Data for estimating soil loss in this study were collected from various sources (see **Table 2**). Landsat 8 satellite imagery was collected from the United States Geological Survey (USGS) portal to extract the influence of vegetation cover in the watershed area. Moderate Resolution Imaging Spectroradiometer (MODIS) satellite imagery was obtained from the Earth Observing System Data and Information System (EOSDIS) to measure the effectiveness of human actions in reducing erosion. Rainfall data were obtained from Climate Hazards Infra-Red Precipitation with Station data (CHIRPS) imagery,

Table 2: Data description for soil erosion modelling in the Poleang River Basin

Variable	Data Type	Spatial Grid	Acquisition Period	Sources
Satellite image	Landsat 8	30 m	2024	United States Geological Survey
	MODIS Land Cover Type (MCD12Q1) ver 6.1	500 m	2023	Earth Observing System Data and Information System
Rainfall data	CHIRPS	5.5 km	1994-2024	Climate Hazards Group
Soil properties	USDA	-	-	FAO-USDA
Topographic data	DEM SRTM	30 m	2000	United States Geological Survey

a high-resolution quasi-global rainfall dataset. Monthly/annual rainfall data from 1994 to 2024 were used to measure the potentially damaging power of rainfall on the soil. Soil data obtained from the Food and Agriculture Organization (FAO) was used to measure the level of vulnerability or resistance of the soil to the release and transport of soil particles by water. This helps predict the amount of erosion based on soil characteristics such as texture, organic matter, structure, and permeability. Meanwhile, Shuttle Radar Topography Mission (SRTM) Digital Elevation Model (DEM) data were used to measure the effect of slope length (L) and slope (S) on the magnitude of soil erosion. These factors determine the potential for greater surface runoff and accelerate erosion on steep and long slopes.

2.3. Erosion Model

2.3.1. USLE Model

This model was introduced to estimate soil erosion rates (**Wischmeier & Smith, 1978, 1965**). The USLE model is typically analyzed using GIS and has been widely adopted worldwide. This basic model relies heavily on rainfall patterns, land use, topography, soil erodibility, and anti-erosion practices, and is written as the following **Equation 1**:

$$A_{USLE}=R \times K \times L \times S \times C \times P \quad (1)$$

where A is average soil loss (t/ha^{-1}/year^{-1}); R is rainfall-runoff erosivity factor (MJ mm/ha^{-1}/h^{-1}/year^{-1}); K is the soil erodability factor (t ha h/ha^{-1}/MJ^{-1}/mm^{-1}); L is the slope length factor (dimensionless); S is the slope gradient factor (dimensionless); C is the cropping management factor; and P is supporting conservation practice factor (dimensionless, ranging 0 to 1).

2.3.2. MUSLE Model

The MUSLE model (**Williams, 1975**) is a modified version of the USLE model (**Wischmeier & Smith, 1965**). In this framework, the R factor is substituted with variables representing total runoff volume and peak discharge rates to estimate soil loss. The MUSLE model calculates the average soil loss caused by flooding through the product of the flood volume (V in m^3), the peak flood discharge (q_p in m^3/s), the soil erodibility (K), the slope index (S), the slope length (L), the vegetation cover (C), and the cultural practices (P). This model is written with the following **Equation 2**:

$$A_{MUSLE} = 11.8(Q \times q_p)^{0.56} \times K \times LS \times C \times P \quad (2)$$

2.3.3. RUSLE Model

The RUSLE model places greater emphasis on calculating average annual soil loss, a revision of the USLE equation (**Wischmeier & Smith, 1978, 1965**). In terms of environmental management, this model is particularly effective at quantifying complex erosion types, specifically gully and intergully degradation. The RUSLE model has been widely applied to river basins worldwide (**Aldiansyah & Wardani, 2024; da Cunha et al., 2017; Djoukbala et al., 2018; Markose & Jayappa, 2016; Tetford et al., 2017; Toubal et al., 2018; Wijesundara et al., 2018**). This model is written through the following **Equation 3**:

$$A_{RUSLE}=R \times K \times LS_{2D} \times C \times P \quad (3)$$

where R is the rainfall-runoff erosivity, K is the soil erodibility factor, LS_{2D} is the 2D topography factor derived from DEM flow accumulation, P is the anti-erosion practice and C is the vegetation cover factor.

2.4. Factors of Models

2.4.1. R factor

The R factor shows the pressure of raindrops on the soil surface at a certain intensity scale. This factor indicates the intensity of particles that can be transported when raindrops break up surface aggregates. Although many factors are used to estimate the effect of rainwater runoff, this factor is the most well-known. The R factor assesses the rainfall erosion index by understanding the influence of rainfall kinetic energy, soil particle disaggregation, and surface compaction, and its maximum intensity, while also determining when the infiltration capacity of surface runoff occurs.

2.4.1.1. Rainfall erosivity factor (R) according to MUSLE

This factor is estimated from the runoff volume and peak flow (**Williams & Berndt, 1977**). Peak flow is calculated assuming that rainfall has uniform intensity throughout the area, using the following **Equation 4**:

$$R=11.8(Q \times q_p)^{0.56} \quad (4)$$

where Q is the volume of runoff (m^3); q_p is peak flow rate (m^3 s^{-1}).

The measured runoff volume and peak flow in this study were recorded at the hydrometric post on the Poleang River.

2.4.1.2. Rainfall erosivity factor (R) according to RUSLE and USLE

Estimating the R factor in the basic model requires information on the kinetic energy (Ec) and the 30-minute average intensity (I30) of raindrops (**Wischmeier & Smith, 1965**). In the study area, only CHIRPS data provide complete monthly and annual average values. This study uses an alternative formula that only includes monthly and annual rainfall to determine the R factor

Table 3: Estimation of K factor in the Poleang River Basin

Soil	ms (sand) topsoil %	msilt (silt) topsoil %	mc (clay) topsoil %	orgC Organic carbon %	f_{csand}	$f_{cl\text{-}si}$	f_{orgc}	f_{hisand}	K_{USLE}	K
Ao	53.6	15.8	30.6	2.25	0.168	0.998	0.724	0.975	0.1186	0.0156
Lc	64.3	12.2	23.5	0.63	0.176	0.983	0.725	0.998	0.1248	0.0164
Je	70.8	12.8	16.5	1.15	0.174	0.942	0.780	0.988	0.1267	0.0167

Ao = Orthic Acrisols, Lc = Chromic Luvisols, Je = Eutric Fluvisols

(**Cormary & Masson, 1964**). **Equation 5** is written as follows:

$$logR=1.74log\sum_{i=1}^{12}\frac{P_i^2}{P}+1.29, \quad (5)$$

where R is rainfall erosivity (MJ mm ha^{-1}/h^{-1}/year^{-1}); P_i is the monthly precipitation (mm), and P is the annual precipitation (mm). The R value is applied to the entire region using inverse distance weighting geostatistics.

2.4.2. K factor

The K-factor quantifies soil erodibility, specifically measuring the soil's inherent capacity to withstand the erosive forces of precipitation and surface discharge. It reflects how soil characteristics influence the overall rate of land degradation through the interplay of runoff, rainfall, and seepage. The calculation of this index is primarily derived from the soil's physical composition, including its organic content and textural fractions like silt, sand, and clay.

Given the lack of accurate soil maps, we used soil maps issued by the United States Department of Agriculture to determine the required soil parameters. This data is the result of a collaboration between the FAO and the USDA. The World Harmonized Soil Database is a 30-degree arc framework consisting of over 15,000 characteristic units. This data consists of 21,600 rows and 43,200 columns that have been linked to harmonized soil properties. The use of a standardized structure allows for better association of data with unit structure and soil parameter descriptions (**FAO & ISRIC, 2012**). Soil erodibility values are calculated using the following **Equation 6** (**Neitsch et al., 2011**):

$$K_{USLE}=K_w=f_{csand}\cdot f_{cl\text{-}si}\cdot f_{orgc}\cdot f_{hisand} \quad (6)$$

where f_{csand} represents a parameter that attenuates the K-factor in soil profiles with high coarse-sand content, while raising it for textures where sand is scarce; $f_{cl\text{-}si}$ coefficient indicates a reduction in the erodibility factor for soils exhibiting a high ratio of clay to silt; f_{orgc} is applied to lower the K-values as the concentration of organic matter increases; f_{hisand} serves to minimize the K-value specifically for soils that are predominantly composed of sand. The texture of the four factors above is calculated using **Equations 7** to **10** below.

$$f_{csand}=\left(0.2+0.3\cdot exp\left[-0.256\cdot m_s\cdot\left(1-\frac{m_{silt}}{100}\right)\right]\right), \quad (7)$$

$$f_{cl\text{-}si}=\left(\frac{m_{silt}}{m_c+m_{silt}}\right), \quad (8)$$

$$f_{orgc}=\left(1-\frac{0.25\cdot orgC}{orgC+exp[3.72-2.95\cdot orgC]}\right), \quad (9)$$

$$f_{hisand}=\left(1-\frac{0.7\cdot\left(1-\frac{m_s}{100}\right)}{\left(1-\frac{m_s}{100}\right)+exp\left[-5.51+22.9\cdot\left(1-\frac{m_s}{100}\right)\right]}\right), \quad (10)$$

where m_s is the percentage of sand content consisting of particles with a diameter between 0.05 and 2.00 mm; m_{silt} is the percentage of silt content, which includes particles ranging from 0.002 to 0.05 mm in diameter; m_c is defined as the percentage of clay content for particles smaller than 0.002 mm; $orgC$ is the percentage of organic carbon content found within the specific soil layer (see **Table 3**).

2.4.3. LS factor

This factor is one of the key factors in water erosion. Slope gradient plays a crucial role in the processes of soil release, transport, and deposition. This factor is manifested in slope length (L) and slope degree (S). Crucially, the mathematical formulation of the LS factor fundamentally differs between the USLE and the RUSLE models; the former relies on plot parameters, whereas the latter integrates a two-dimensional terrain approach tailored. These two sub-factors are recommended to be used together to evaluate the influence of slope gradient on overall erosion rates. These sub-factors are determined from the Digital Terrain Model (DTM) of the SRTM DEM. Our study uses three equations that fit the model. The LS factor for USLE is calculated by **Equations 11** to **13**, MUSLE by **Equations 14** and **15**, and RUSLE by **Equation 16** below.

2.4.3.1. USLE-based LS component

$$LS=\left(flow\ accumulation\times\frac{resolution}{22.1}\right)^m\times$$

$$\times\left(65.41\ sin^2\theta+4.56sin\theta+0.065\right), \quad (11)$$

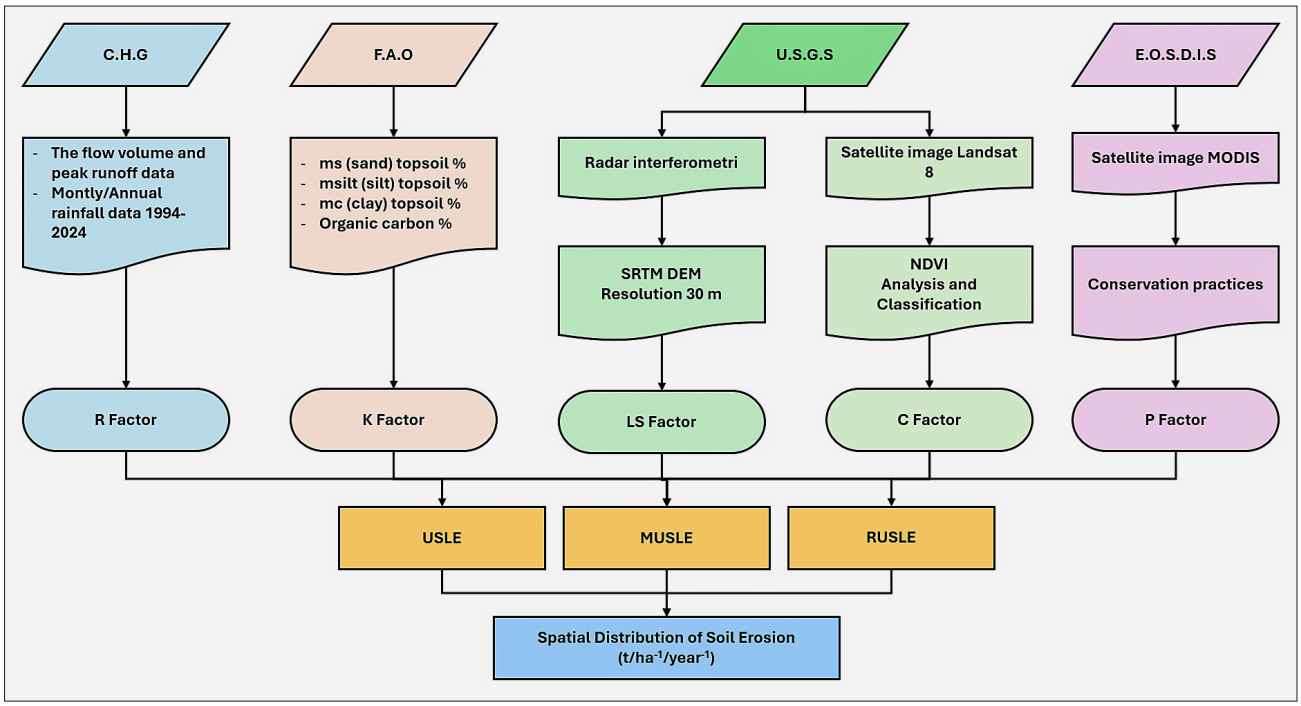


Figure 2: Flowchart of the methodology

$$m=0.6 \times \left[1\text{-}e^{(\text{-}35.835 \times S}\right], \quad (12)$$

$$\theta=tan^{-1}\left(\frac{S}{100}\right) \quad (13)$$

where S is the field slope (%), and θ is the field slope steepness in degrees. Since the analysis was performed in a GIS raster format, the original discrete USLE m exponent values were adapted to continuous using the **Nearing et al.** (**1989**) approach, while retaining the original USLE S factor equation.

2.4.3.2. MUSLE-based LS parameter

$$LS=1.4 \times \left(\frac{A_s}{22.1}\right)^{0.4} \times \frac{sin\,(\theta \times 0.01745)^{1.4}}{0.09} \quad (14)$$

$$A_s=flow\ accumulation\ \times resolution, \quad (15)$$

The value of A_s represents the product of the flow accumulation and the specific spatial resolution used in the model.

2.4.3.3. RUSLE-based LS variable

$$LS=\left(flow\ accumulation \times \frac{resolution}{22.1}\right)^{m} \times$$

$$\times\,(0.065+0.045 \times S+0.0065 \times S^2) \quad (16)$$

where S is the slope angle (%), m is assigned based on the degree of slope (**Wischmeier & Smith, 1978**), ranging from 0.2 for gradients below 1% to 0.5 for steeper slopes exceeding 5%.

2.4.4. C factor

Plant cover is essential for mitigating the impact of water-driven soil degradation by reducing runoff velocity. According to (**Kalman, 1967**), vegetation is even the second most important factor in controlling soil erosion risk. Numerous studies have estimated this factor from the Normalized Difference Vegetation Index (NDVI) to assess soil erosion (**Lin et al., 2002; Wang et al., 2002**). This algorithm can be applied through regression models, field studies, guide boards, or remote sensing to assess correlations. The unknown value of this factor is estimated from an equation obtained from a linear regression analysis.

NDVI values generally range from -1 to +1. Negative values are more representative of surfaces without plant cover, such as water or clouds, and snow, where red reflectance tends to be greater than near-infrared (**Souidi et al., 2014**). Bareland also exhibits a similar trend, given that the resulting order of magnitude is nearly identical for both reflectances, which approach zero. Meanwhile, vegetation formation has positive values in the range of 0.1 to 0.5, with the densest vegetation indicating the highest values.

The C factor was calculated using NDVI values generated from 30 m resolution Landsat 8 imagery. By comparing red and infrared band reflectance, this study characterizes the relationship between vegetation characteristics and soil erosion, highlighting the protective role of different land covers. The C factor value in this study

used a linear inverse transformation that follows the general NDVI-C relationship, so that higher vegetation density will provide greater soil protection (**Karaburun, 2010**). Factor C is calculated using the following **Equation 16**.

$$C = 1.1504 - 1.4546 \times NDVI \quad (16)$$

2.4.5. P factor

This factor represents conservation practices for water erosion. Its value tends to vary depending on the conservation techniques adopted. In this assessment, the support practice factor (P) was assigned a value of 1 for the whole area. This decision reflects the absence of existing anti-erosion techniques in the field, as the P factor scale ranges from 1 (no conservation) to 0 (maximum protection). A general overview of how the model works is presented in **Figure 2**.

3. Results and Discussion

3.1. R factor

The erosion map generated from CHIRPS data was used to evaluate the R-factor value in the Poleang River Basin, which varies from 1806 to 2366 MJ mm/ha^{-1}/h^{-1}/year^{-1} (see **Figure 3**). The identified values are in the northern part of the area, while the lowest values were recorded in the southern part. The R-factor is distributed throughout the area, with the highest erosion located in the northern side with an R-value of 2,199 to 2,366 MJ mm/ha^{-1}/h^{-1}/year^{-1}. The low erosion class is in the range of 1,806 to 1,927 MJ mm/ha^{-1}/h^{-1}/year^{-1}, affecting 28.25% of the surface. Meanwhile, about 17.15% represents moderate erosion with an R-factor ranging from 2,019 to 2,116 MJ mm/ha^{-1}/h^{-1}/year^{-1}.

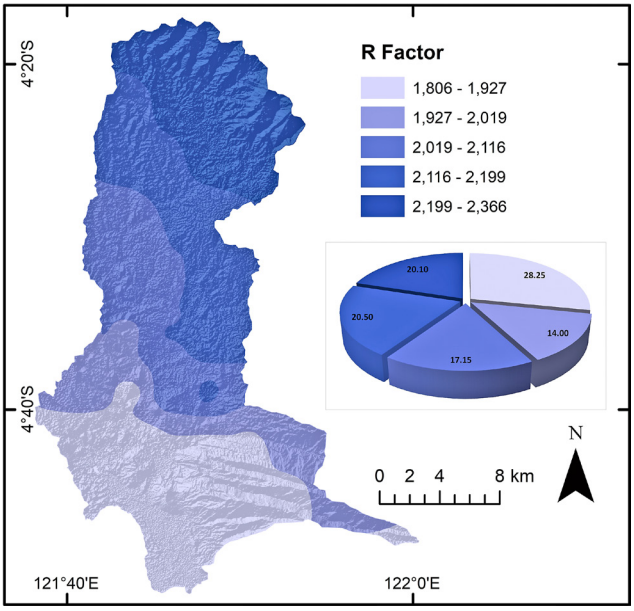


Figura 3: R-factor of soil erosion

3.2. K factor

The erodibility of soils throughout the Poleang River Basin is characterized by K-factor values spanning from 0.0156 to 0.0166 MJ mm/ha^{-1}/h^{-1}/year^{-1}. These three soil types (Ao, Lc, and Je) have high erodibility due to their weak aggregate stability, low permeability in the lower horizons, and the presence of fine sediments (silt/fine sand) that make them easily transported by runoff. **Borrelli et al. (2017)** also reported the same thing, where these soil types are very sensitive to surface runoff erosion. The distribution map of the composite K factor shows the spatial erodibility of the three soil groups (see **Figure 4**). Spatial analysis of the watershed reveals that nearly 37% of the area exhibits erodibility values below 0.015, whereas a smaller portion of approximately 3% falls within the higher K-factor range of 0.015 to 0.016 (see **Figure 3**). The resulting digital map provides researchers with the capability to perform pixel-level manipulations across the entire basin surface.

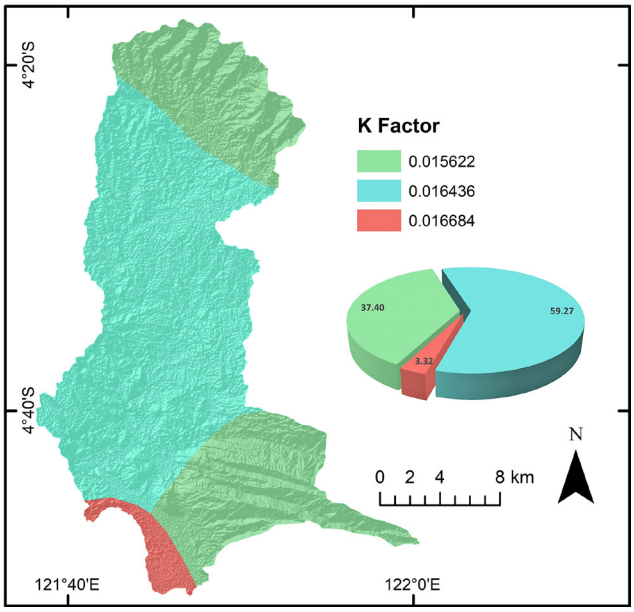


Figure 4: K-factor of soil erosion

3.3. LS factor

To establish a robust topographic baseline for the LS factor evaluation, a standalone slope gradient map was generated from the 30-m resolution DEM (see **Figure 5**). The geomorphological structure of the Poleang River Basin is characterized by highly heterogeneous terrain. The low-lying downstream areas are predominantly dominated by flat to gently sloping terrains (0–8%), which provide depositional zones for transported sediments. Conversely, the upper catchment headwaters exhibit severe terrain dissection, featuring steep (25–45%) and very steep (>45%) slope gradients. These high-gradient upper sectors exert a primary geometric control on soil erosion mechanics by significantly accelerating sur-

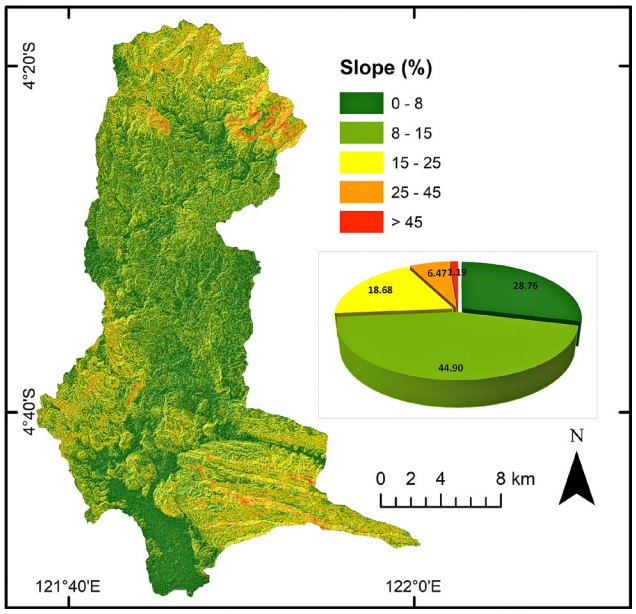


Figure 5: Slope gradien factor

face runoff velocity and increasing transport capacity, directly inflating the calculated local LS factor values.

The LS factors generated by the USLE, MUSLE, and RUSLE models varied between 1.70 and 8025.08, 1.70 and 6307.60, and 1.70 and 9599.76, respectively (see **Figure 6; Table 4**). The maximum and minimum erosion ratios were applied to steep slopes (25-45%) and gentle slopes (0-8%), respectively, with the same ratio of 8:24:12. Considering the ratios, the highest erosion values were obtained from the RUSLE model. However, given its linear nature, changes in a single factor will affect analogous changes in the LS value effect.

High LS values are located in the upstream and in hills with varying elevations. Meanwhile, low LS values are distributed in the lowlands and riverbeds. This distribution clearly confirms that the river basin is highly susceptible to erosive processes across all segments of the longitudinal profile. This finding is consistent with numerous studies (**Abdo & Salloum, 2017; da Cunha et al., 2017; Djoukbala et al., 2018; Imamoglu & Dengiz, 2017**). This pattern also aligns with **Pham et al. (2018)** findings that erosion increases exponentially with increasing slope gradient. Furthermore, as the slope gradient increases, the kinetic energy of rainfall remains constant, while downstream transport increases due to the increased kinetic energy of runoff (**Thomas et al., 2018a**).

3.4. C factor

The spatial distribution of the cover management factor (C) in this study is derived from the NDVI analysis.

Table 4: Proportional coverage of soil erosion categories as estimated by three different modelling frameworks

USLE			MUSLE			RUSLE		
LS Class	Area (ha)	Area (%)	LS Class	Area (ha)	Area (%)	LS Class	Area (ha)	Area (%)
1.70 -75.01	66,804.01	59.79	1.70 - 78.12	67,073.10	60.03	1.70 - 76.68	67,103.10	60.06
75.01 -221.07	33,788.70	30.24	78.12 - 244.26	33,185.69	29.70	76.68 - 264.15	33,524.79	30.01
221.07 -623.89	9,473.38	8.48	244.26 - 587.81	9,541.54	8.54	264.15 - 601.58	9,468.54	8.47
623.89 -1497.42	1,613.11	1.44	587.81 - 1183.34	1,872.30	1.68	601.58 - 1576.38	1,573.11	1.41
1497.42 - 8025.08	44.34	0.04	1183.34 -6307.60	50.91	0.05	1576.38 - 9599.76	54.00	0.05

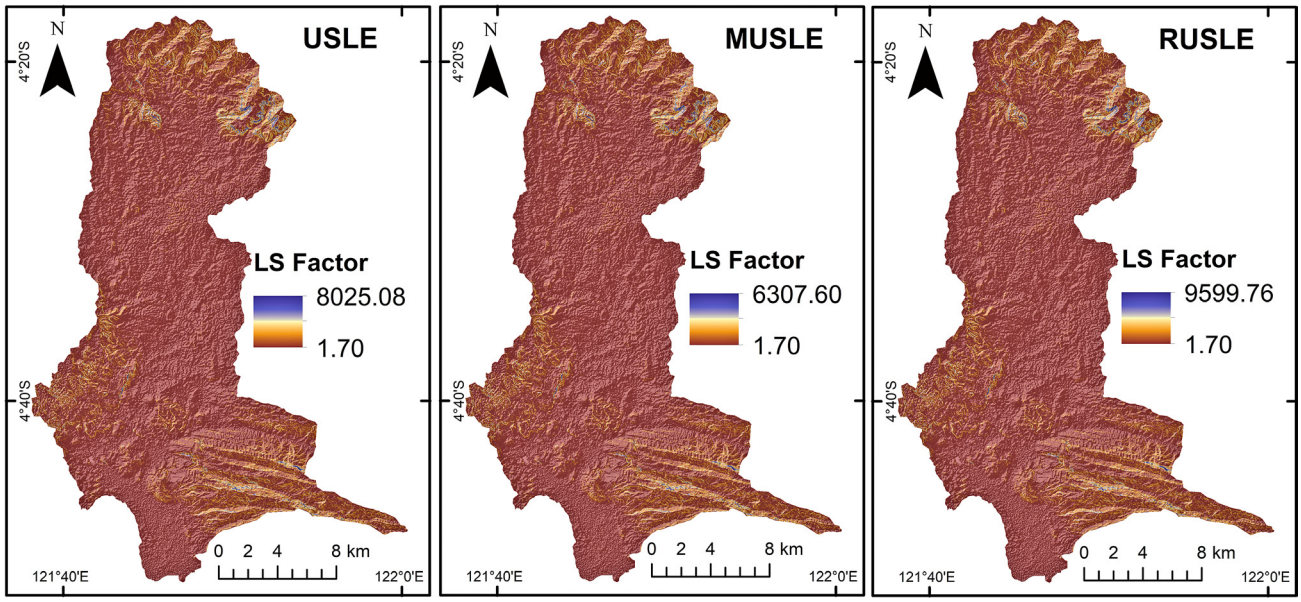


Figure 6: LS-factor of soil erosion

The resulting C values fluctuate within a range of -0.22 to 1.56 (see **Figure 7**). To optimize the spatial presentation of these values, the continuous dataset was categorized into five distinct classes using the Natural Breaks (Jenks) optimization algorithm in GIS, which minimizes variance within each class while maximizing differences between them. Statistical analysis of this data reveals that approximately 72.78% of the watershed is characterized by sparse vegetation cover, leaving only 27.22% of the territory effectively protected with C values below 0.07. The presence of values slightly outside the strict theoretical boundaries (specifically -0.22 and 1.56) is a direct mathematical artifact of applying the unconstrained linear regression equation to extreme spectral reflectances, such as water bodies/shadows or highly saturated dense canopy pixels. Areas exhibiting high erosion susceptibility due to low vegetation density, such as shrubs, degraded open lands, and active agricultural fields, frequently show higher C values. Conversely, indices below the 0.07 threshold are more indicative of dense forests and well-established plantations. Values ranging from 0.5 to 0.9 are typically associated with low-density cover types, including sparse woodlands and light shrubbery, while the highest values are found in deforested zones or post-harvest agricultural land.

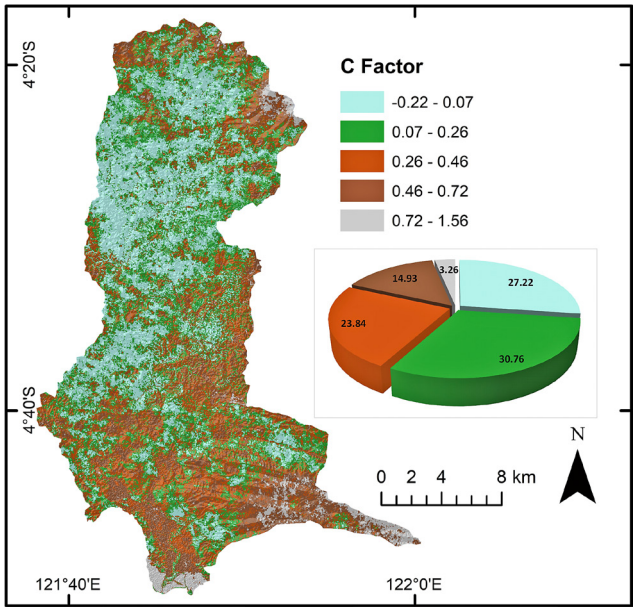


Figure 7: C-factor of soil erosion

3.5. *Assessment and evaluation of soil erosion*

We calculated the annual average value of soil loss in the Poleang River Basin with the USLE, MUSLE, and RUSLE models based on **Equations 1**, **2**, and **3**. To generate the erosion potential map, five distinct environmental parameters were integrated using a raster-stacking technique within the ArcGIS environment, maintained at a 30 m spatial resolution. The results were then compared with the erosion map issued by the Ministry of Environment and Forestry of the Republic of Indonesia (KLHK). To maintain local policy relevance and standardization, the continuous soil loss values (t/ha^{-1}/year^{-1}) were categorized into five discrete hazard classes following the national regulatory framework established by the KLHK (**PERDIRJEN-BPDASPS, 2013**). These standard threshold ranges classify soil loss rates < 15 (Very Slight), 15–60 (Slight), 60–180 (Moderate), 180–400 (Severe), and >400 (Very Severe) erosion risk. To facilitate practical land rehabilitation programs and administrative coordination, the study area was delineated into 6 sub-district zones. Furthermore, to capture the topographical variance within each administrative unit, each sub-district was further divided into two operational landscape zones: the upstream and downstream sectors. Zonal statistics were then used to extract the mean annual soil loss percentage for each sector, resulting in 12 distinct spatial data pairs utilized for the power regression analysis.

3.5.1. USLE Model

According to the USLE model simulation, the total annual sediment yield in the study area reaches 2.81 × 10^{7} t/year^{-1}, which corresponds to a specific erosion rate of 252 t/ha^{-1}/year^{-1}. The spatial distribution (see **Figure 8a**) demonstrates a wide variance in water-driven erosion, ranging from 0 to 400 t/ha^{-1}/year^{-1} across the basin. High-risk zones are predominantly concentrated on hilly terrains and steep embankments characterized by susceptible soil substrates. Quantitatively, these high-vulnerability regions encompass 81.69% of the Poleang River Basin. In contrast, the remaining 18.31% of the landscape is classified as having low erosional sensitivity (see **Table 5**).

3.5.2. MUSLE Model

The MUSLE simulation yielded results consistent with the USLE estimates, showing a total annual sediment discharge of 2.35 × 10^{7} t/year. This translates to a specific erosion rate of 210 t/ha^{-1}/year^{-1} (see **Figure 8b**). A detailed breakdown of the area's distribution across various erosion risk categories is presented in **Table 5**.

3.5.3. RUSLE Model

The risk map from the RUSLE model shows a slightly different pattern from the MUSLE model, but the results are similar to those of the USLE (see **Figure 8c**). This result is also consistent with the findings of **Romdania & Herison (2024)** that the USLE and RUSLE models show similar patterns, while the MUSLE model shows a wider dispersal of potential risks than the other models. The estimated annual soil degradation for this model reaches a total of 2.57 × 10^{7} t/year, which represents a specific intensity of 230 t/ha^{-1}/year^{-1}. A comprehensive breakdown of these erosion risk categories is detailed in **Table 5**.

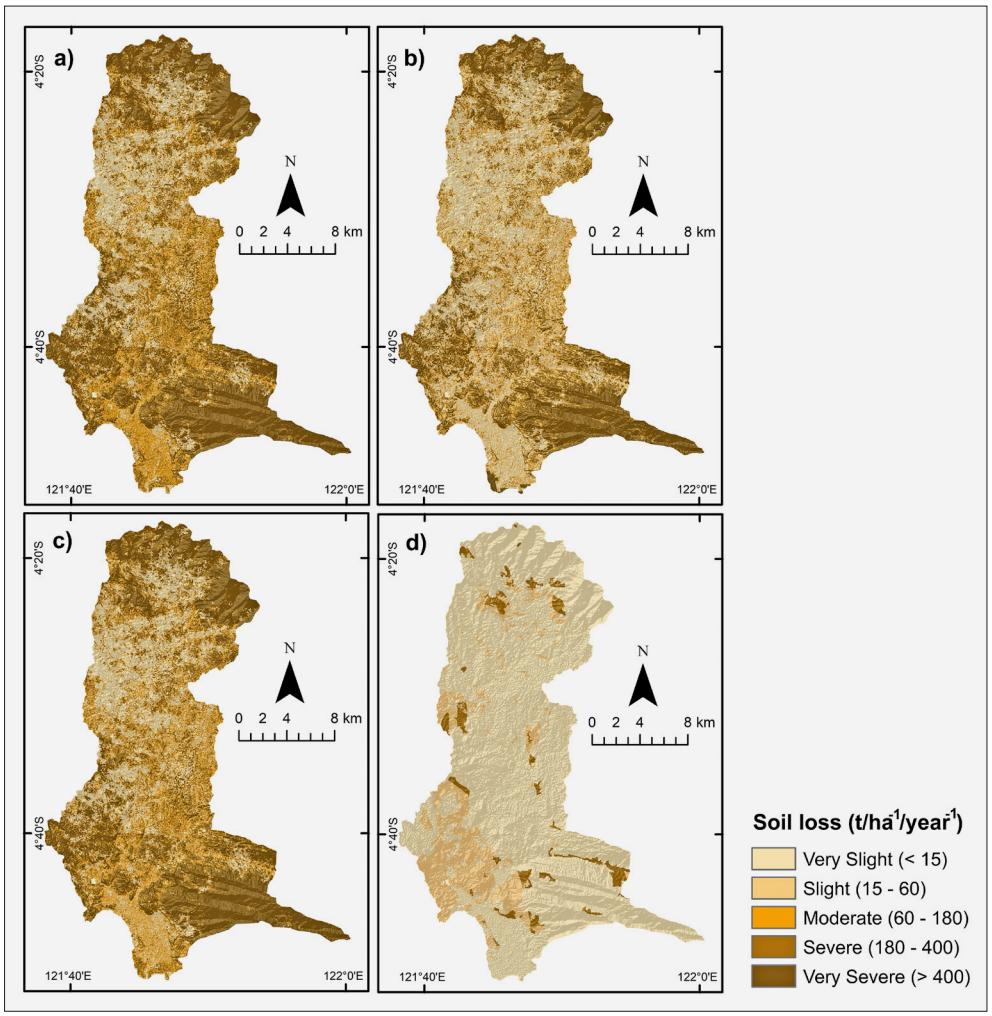


Figure 8: Soil erosion map in the Poleang River Basin: a) USLE, b) MUSLE, c) RUSLE, and d) KLHK models

Table 5: Distribution of land area across various soil erosion severity levels by three models

Class	USLE		MUSLE		RUSLE	
	Area (ha)	%	Area (ha)	%	Area (ha)	%
Very slight	20,457.27	18.31	28,069.60	25.12	21,856.86	19.56
Slight	12,000.87	10.74	21,042.09	18.83	15,997.50	14.32
Moderate	21,968.55	19.66	15,684.84	14.04	22,404.24	20.05
Severe	17,825.94	15.96	13,712.58	12.27	16,684.47	14.93
Very severe	39,470.91	35.33	33,214.43	29.73	34,780.47	31.13

Severe erosion rates were observed in hilly areas and on steep slopes, compared to the KLHK map. The KLHK model (see **Figure 8d**) tends to be more conservative, while our three models tend to be more contractive. Many areas fall into the Severe to Very Severe category, particularly in the southern and central parts of the watershed. This discrepancy stems from the higher precision of our input data, utilizing a 30 m SRTM DEM and 2024 Landsat 8 imagery, which captures localized topographic variations and recent land-cover changes such as deforestation or new agricultural openings that are often generalized in national-scale KLHK datasets. While KLHK focuses on macro-policy mapping, our modelling (particularly MUSLE) integrates dynamic hydrological processes through runoff energy, identifying high-risk hidden hotspots. Consequently, these findings necessitate a formal re-evaluation of official erosion risk maps in the Poleang River Basin to prevent mitigation failures, as current regional policies may significantly underestimate the actual land degradation. This finding is consistent across all models and actual erosion rate reports and indirectly indicates that erosion is quite active in the downstream Poleang River Basin. The calculated erosion rate in this area is at a high erosion index (IE = 1.5), as reported by the regional watershed management agency (**Syaf et al., 2022**). According to na-

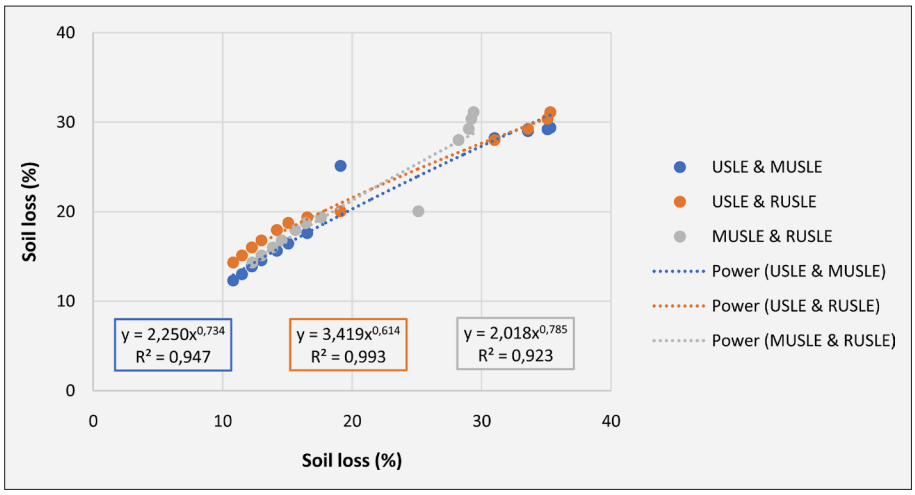


Figure 9: Variation of the erosion calculated by the three models

tional standards, an IE > 1.0 indicates that soil loss exceeds tolerable limits (**Kementerian Kehutanan, 2014**). This condition sufficiently indicates that the Poleang River Basin is experiencing land degradation driven by unsustainable land management, geological vulnerability, and intense hydro-climatic factors, necessitating urgent conservation measures.

The sharp topographic gradient of the Poleang River Basin, which abruptly rises from sea level (0 m) to a peak elevation of 1060 m within a compact basin footprint, plays a critical role in modulating localized hydrometeorological processes. Such geomorphological configurations strongly trigger orographic rainfall enhancement. As moisture-laden air masses are forced upward along the steep windward slopes, adiabatic cooling intensifies, leading to the orographic amplification of precipitation magnitude and intensity in the upper catchment (**Houze, 2012**). This elevation-dependent precipitation variability introduces high spatial heterogeneity in erosive storm events, where the upper slopes are subjected to raindrops with significantly greater kinetic energy, thereby localized inflating the rainfall erosivity factor within the USLE and RUSLE frameworks. Furthermore, this steep topography exerts a profound control on catchment-scale runoff generation. The combination of high-intensity orographic storms and steep slope gradients curtails the time to peak concentration, shifting the dominant hydrological response toward rapid, Hortonian surface runoff. This rapid concentration of flow accelerates peak discharge rates in the upstream channels, directly amplifying the runoff erosivity capacity modelled by the MUSLE framework (**Okiria et al., 2025**). Acknowledging these coupled orographic-topographic feedbacks provides a more nuanced understanding of why the upper sectors of the basin act as critical erosion hotspots, offering vital spatial insights for targeted soil conservation.

This study highlights relatively similar results for the USLE, MUSLE, and RUSLE erosion models. However, the USLE model exhibits a higher spatial risk disputation than the MUSLE and RUSLE models. The fundamental divergence lies in the mechanical representation of the primary energy factors. In the USLE and RUSLE frameworks, the energy is derived from rainfall erosivity, which represents the cumulative kinetic energy of raindrops to detach soil particles. This makes USLE/RUSLE highly sensitive to the tropical rainfall aggressiveness of the Poleang Basin. In contrast, MUSLE replaces the rainfall factor with a runoff energy factor ($Q \cdot q_p \cdot 0.612$). This shift from meteorological energy to hydrological energy allows MUSLE to better simulate the sediment transport capacity of river flows during extreme flood events, which is a critical process in catchment-scale hydrology. Furthermore, the USLE model's reliance on static long-term averages often fails to account for the threshold-breaking energy of surface runoff in steep hilly areas. The RUSLE model, while sharing the rainfall factor with USLE, introduces a more dynamic slope length and steepness factor and a time-varying conservation management factor. In our analysis, the RUSLE model's aggressive results in the southern region (see **Figure 9**) suggest that the topographic energy in the Poleang Basin's rugged terrain significantly amplifies the erosive power of rainfall compared to the more generalized LS calculations used in the KLHK maps. This detailed energy partitioning explains why our empirical results capture severe erosion hotspots that are otherwise buffered in broader national assessments. The conservation management factor is quite effective in the USLE model, which can explain its higher erosion rate. The differences in the results also show relatively close results.

The R^2 obtained among the three calculated models ranged from 0.91 to 0.99 (see **Figure 9**). Statistical validation against KLHK data shows a strong positive correlation with R^2 values ranging from 0.78 to 0.80 (see **Figure 10**). This range indicates a strong correlation between the resulting models. Based on the findings, the RUSLE framework appears to align well with the current dataset. However, this alignment requires careful

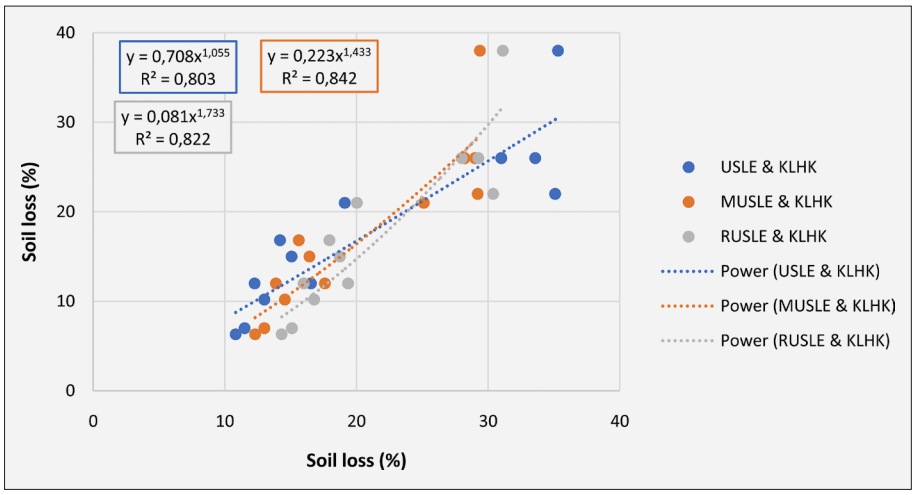


Figure 10: Variation of the erosion calculated by the three models compared to the KLHK model

interpretation, as the model's empirical foundations are inherently tied to the specific geographic and climatic conditions of its origin. In this study, the performance of RUSLE suggests a strong adaptability to Indonesia's tropical landscape. The discrepancies noted among the three models likely stem from variations in how dominant erosive mechanisms are captured across different spatial and temporal dimensions. Since RUSLE was originally calibrated for North American agricultural contexts, its conceptualization of soil loss may differ from the complex dynamics of tropical ecosystems. Nonetheless, these models remain highly practical due to their streamlined data inputs and low computational complexity (**Harmon & Doe, 2012**). A significant challenge arises from the rigid internal structures of these models, which prevent the isolation or modification of specific processes. This lack of flexibility becomes particularly limiting when frameworks calibrated for specific geographic regions or distinct spatial scales are applied to environments with different physical characteristics. In addition, empirical relationships are often calibrated to the data set from which they are derived (**Ghadiri & Rose, 1993; Hudson & Nations, 1993**). Calibrating or developing models is an ideal approach in a regional context, such as the Soil Loss Estimation Model for Southern Africa (SLEMSA) (**Elwell, 1978**), and the European Soil Erosion Model (EUROSEM) (**Hudson & Nations, 1993**).

The results of this study also align with numerous other reported studies on water erosion evaluation conducted in other Indonesian watersheds with similar climate and environmental characteristics, such as the Citarum River Basin at 108.60 t/ha^{-1}/year^{-1} (**Nahib et al., 2024**), the Mrica Reservoir Catchment at 443.90 t/ha^{-1}/year^{-1} (**Cantik et al., 2023**), the Kalikonto watershed at 72 t/ha^{-1}/year^{-1} (**Andriyanto et al., 2015**), and the Roraya River Basin at 307.22 t/ha^{-1}/year^{-1} (**Aldiansyah & Wardani, 2024**).

While the accuracy of empirical soil loss predictions remains a subject of academic debate, this approach continues to be one of the most reliable methodologies available. The findings of this research serve as a strategic framework for regional planners, offering a robust simulation of conservation scenarios. These insights are particularly valuable for designing erosion mitigation strategies in sloped terrains, where hydraulic erosive forces are the primary drivers of land degradation.

Beyond the regional context of the Poleang River Basin, this study contributes to the global discourse on the reliability of national-scale erosion assessments in data-scarce tropical regions. The high correlation (0.78–0.80) between localized high-resolution empirical models and official government maps confirms that while national datasets are useful for macro-level planning, they inherently lack the sensitivity required for local disaster mitigation. While climate change-induced extreme precipitation events inherently amplify soil detachment by increasing raindrop kinetic energy, a phenomenon directly captured by the rainfall erosivity (R factor) in USLE and RUSLE, the integration of MUSLE further refines this by capturing the corresponding surge in peak surface runoff within tropical catchments. Consequently, this multi-model comparative framework offers a scalable and comprehensive methodology for developing nations to evaluate both rainfall-driven and runoff-induced erosion dynamics without solely relying on expensive, long-term field monitoring.

However, our results have the exclusive reliance on the CHIRPS satellite precipitation product for calculating the rainfall erosivity factor, without direct validation against local ground rain gauges. Since the R factor heavily dictates the absolute values of USLE/RUSLE-type models, this reliance introduces spatial uncertainties into the absolute soil loss estimates. However, this method can be an alternative when the severe scarcity and temporal fragmentation of continuous, long-term observational weather stations within the Poleang River Basin. Furthermore, extensive validation studies across various tropical catchments have demonstrated that CHIRPS exhibits high spatial-temporal consistency and

strong correlation with ground-truth BMKG stations, particularly in capturing monthly and annual convective rainfall trends (**Jahanshahi et al., 2024; Liu et al., 2020**). While the absolute erosion tonnage should be interpreted with caution due to this systemic satellite uncertainty, the model remains robust for identifying macro-level erosion hotspots and spatial variations. Future works should integrate localized automatic weather stations (AWS) to systematically recalibrate the satellite-derived R factor at the catchment scale.

In addition to precipitation data uncertainties, a prominent limitation of this study is the lack of empirical ground-truth validation against measured sediment yield, suspended sediment concentration, or field plot data. While the high statistical correlations demonstrate strong mathematical consistency and conceptual alignment among the USLE, MUSLE, and RUSLE frameworks, they do not substitute for physical validation. This uncertainty is particularly relevant in cultivated or managed agricultural zones, where anthropogenic land disturbances and local conservation practices heavily alter soil vulnerability, potentially leading to over- or under-estimations by empirical models.

4. Conclusions

A primary obstacle in assessing water erosion risk is the scarcity and precision of field data, especially within extensive, ungauged watersheds. This study demonstrates that empirical models, bolstered by advanced GIS capabilities, provide an effective solution to these data constraints. The application of USLE, MUSLE, and RUSLE frameworks in the Poleang River Basin yielded comparable results, with specific soil loss rates of 252 t/ha^{-1}/year^{-1}, 210 t/ha^{-1}/year^{-1}, and 230 t/ha^{-1}/year^{-1}, respectively. High-risk zones were predominantly mapped across hilly and high-gradient terrains. These findings underscore a critical state of land degradation, driven by the synergistic impact of suboptimal land management, geological fragility, and high rainfall erosivity. However, due to data scarcity, the derived erosion rates lack direct validation against physical sediment yield or suspended sediment data.

This study further highlights that the transition from rainfall-based (USLE/RUSLE) to runoff-based (MUSLE) energy factors provides a more dynamic understanding of catchment-scale hydrological processes, particularly in capturing sediment transport during extreme events. While all models show a strong correlation with official KLHK data (R^2 = 0.78–0.80), the higher resolution and updated 2024 parameters in our modelling reveal critical erosion hotspots that are often underestimated in national-scale assessments. Therefore, this study emphasizes that MUSLE is more suitable for event-based sediment mitigation, while RUSLE offers superior precision for long-term land-use planning in tropical ecosystems. The three model mapping output provides a foundational reference for spatial prioritization in land management. By analyzing both the integrated erosion rates and the individual contributions of each factor, stakeholders can more accurately identify critical zones for targeted soil conservation and strategic revegetation programs. The significant discrepancy between our findings and existing regional maps necessitates a formal re-evaluation of official erosion risk boundaries in the Poleang River Basin to ensure effective land-degradation neutrality. Furthermore, this research validates that advancements in geospatial technology and remote sensing significantly enhance the precision of erosion modelling. These tools establish a versatile and scalable methodology for optimizing land preservation policies, particularly in other tropical watersheds where primary field data is limited. Therefore, while these outputs are highly valuable for localized zoning and land rehabilitation planning, the absolute tonnage rates should be interpreted with caution, highlighting the urgent need for future field-scale monitoring in tropical managed catchments.

Acknowledgement

The authors would like to thank the Dean of the Faculty of Teacher Training and Education, as well as the Geography Education Laboratory, Halu Oleo University, for facilitating this research. We also extend our gratitude to the institutions and platforms providing open access data.

Funding

This research was not funded by any funding.

5. References

Abdo, H., & Salloum, J. (2017). Spatial assessment of soil erosion in Alqerdaha basin (Syria). *Modeling Earth Systems and Environment*, *3*(1), 26. https://doi.org/10.1007/s40808-017-0294-z

Aldiansyah, S., & Wardani, F. (2024). Spatiotemporal dynamic of soil erosion in the Roraya River Basin based on RUSLE model and Google Earth Engine. *Journal of Hydroinformatics*, *26*(6), 1273–1294. https://doi.org/10.2166/hydro.2024.219

Andriyanto, C., Sudarto, S., & Suprayogo, D. (2015). Estimation of soil erosion for a sustainable land use planning: RUSLE model validation by remote sensing data utilization in the Kalikonto watershed. *Journal of Degraded and Mining Lands Management*, *3*(1), 459–468. https://doi.org/10.15243/jdmlm.2015.031.459

Bangash, R. F., Passuello, A., Sanchez-Canales, M., Terrado, M., López, A., Elorza, F. J., Ziv, G., Acuña, V., & Schuhmacher, M. (2013). Ecosystem services in Mediterranean river basin: Climate change impact on water provisioning and erosion control. *Science of The Total Environment*, *458–460*, 246–255. https://doi.org/10.1016/j.scitotenv.2013.04.025

Bera, A. (2017). Assessment of soil loss by universal soil loss equation (USLE) model using GIS techniques: a case study of Gumti River Basin, Tripura, India. *Modeling Earth Systems and Environment*, *3*(1), 29. https://doi.org/10.1007/s40808-017-0289-9

Beasley, D. B., Huggins, L. F., & Monke, E. J. (1980). ANSWERS: A Model for Watershed Planning. *Transactions of the ASAE*, *23*(4), 0938–0944. https://doi.org/10.13031/2013.34692

Borrelli, P., Robinson, D. A., Fleischer, L. R., Lugato, E., Ballabio, C., Alewell, C., Meusburger, K., Modugno, S., Schütt, B., Ferro, V., Bagarello, V., Oost, K. Van, Montanarella, L., & Panagos, P. (2017). An assessment of the global impact of 21st century land use change on soil erosion. *Nature Communications*, *8*(1), 2013. https://doi.org/10.1038/s41467-017-02142-7

Bryan, K., & Albritton, C. C. J. (1944). Soil Phenomena as Evidence of Climatic Changes. *Soil Science*, *57*(2).

Cantik, B. K. P., Putra, R., Sapan, E. G. A., Legono, D., & Afifah, K. N. (2023). Assessment of Soil Loss Using RUSLE Method in Mrica Reservoir Catchment, Central Java, Indonesia. *LIMNOTEK Perairan Darat Tropis Di Indonesia*, *29*(2), 1–8. https://doi.org/10.55981/limnotek.2023.2210

Chiew, F. H. S., Whetton, P. H., McMahon, T. A., & Pittock, A. B. (1995). Simulation of the impacts of climate change on runoff and soil moisture in Australian catchments. *Journal of Hydrology*, *167*(1–4), 121–147. https://doi.org/10.1016/0022-1694(94)02649-V

Cormary, Y., & Masson, J. (1964). Etude de conservation des eaux et du sol au Centre de Recherches du Génie Rural de Tunisie : application à un projet-type de la formule de perte de sols de Wischmeier. *Cahiers ORSTOM. Série Pédologie*, *2*, 3–26.

da Cunha, E. R., Bacani, V. M., & Panachuki, E. (2017). Modeling soil erosion using RUSLE and GIS in a watershed occupied by rural settlement in the Brazilian Cerrado. *Natural Hazards*, *85*(2), 851–868. https://doi.org/10.1007/s11069-016-2607-3

Djoukbala, O., Hasbaia, M., Benselama, O., & Mazour, M. (2019). Comparison of the erosion prediction models from USLE, MUSLE and RUSLE in a Mediterranean watershed, case of Wadi Gazouana (NW of Algeria). *Modeling Earth Systems and Environment, 5*(2), 725-743. https://doi.org/10.1007/s40808-018-0562-6

Djoukbala, O., Mazour, M., Hasbaia, M., & Benselama, O. (2018). Estimating of water erosion in semiarid regions using RUSLE equation under GIS environment. *Environmental Earth Sciences*, *77*(9), 345. https://doi.org/10.1007/s12665-018-7532-1

Elaloui, A., Marrakchi, C., Fekri, A., Maimouni, S., & Aradi, M. (2017). USLE-based assessment of soil erosion by water in the watershed upstream Tessaoute (Central High Atlas, Morocco). *Modeling Earth Systems and Environment*, *3*(3), 873–885. https://doi.org/10.1007/s40808-017-0340-x

Elwell, H. A. (1978). Modelling soil losses in Southern Africa. *Journal of Agricultural Engineering Research*, *23*(2), 117–127. https://doi.org/10.1016/0021-8634(78)90043-4

FAO, & ISRIC. (2012). *Harmonized world soil database*.

Gandri, L., Syaf, H., Abadi, M., Hasani, U. O., Arif, L. O. K., & Albasri. (2023). Analisis Daya Dukung Tata Air untuk Monitoring Kinerja Pengelolaan DAS Poleang, Sulawesi Tenggara. *Al-Ard: Jurnal Teknik Lingkungan*, *8*(2), 91–100. https://doi.org/10.29080/alard.v8i2.1731

Ghadiri, H., & Rose, C. W. (1993). Water Erosion Processes and the Enrichment of Sorbed Pesticides. Part 2. Enrichment Under Rainfall Dominated Erosion Process. *Journal of Environmental Management*, *37*(1), 37–50. https://doi.org/10.1006/jema.1993.1003

Harmon, R. S., & Doe, W. W. (2012). *Landscape Erosion and Evolution Modeling*. Springer Science & Business Media.

Houze, R. A. (2012). Orographic effects on precipitating clouds. *Reviews of Geophysics, 50*(1). https://doi.org/10.1029/2011RG000365

Hudson, N., & Nations, F. A. O. U. (1993). *Field Measurement of Soil Erosion and Runoff* (Number 68). Food and Agriculture Organization of the United Nations.

Ikhwali, M. F., Rau, M. I., Nur, S., Ferijal, T., Prayogo, W., & Saputra, S. F. D. (2022). Application of Soil and Water Assessment Tool in Indonesia – a review and challenges. *Desalination and Water Treatment*, *277*, 105–119. https://doi.org/10.5004/dwt.2022.29018

Imamoglu, A., & Dengiz, O. (2017). Determination of soil erosion risk using RUSLE model and soil organic carbon loss in Alaca catchment (Central Black Sea region, Turkey). *Rendiconti Lincei*, *28*(1), 11–23. https://doi.org/10.1007/s12210-016-0556-0

Jahanshahi, A., Roshun, S. H., & Booij, M. J. (2024). Comparison of satellite-based and reanalysis precipitation products for hydrological modeling over a data-scarce region. *Climate Dynamics, 62*(5), 3505–3537. https://doi.org/10.1007/s00382-023-07078-x

Kalman, R. (1967). *Essai d'évaluation pour le pré-Rif du facteur couverture végétale de la formule de Wischmeier de calcul de l'érosion*.

Karaburun, A. (2010). Estimation of C factor for soil erosion modeling using NDVI in Buyukcekmece watershed. *Ozean Journal of Applied Sciences*, *3*(1), 77–85.

Kementerian Kehutanan. (2014). *Peraturan Menteri Kehutanan Nomor P.61/Menhut-II/2014 tentang Pedoman Teknis Monitoring dan Evaluasi Pengelolaan Daerah Aliran Sungai*.

Kinnell, P. (2001). Slope length factor for applying the USLE-M to erosion in grid cells. *Soil and Tillage Research*, *58*(1–2), 11–17. https://doi.org/10.1016/S0167-1987(00)00179-3

Knisel, W. G. (Ed.). (1980). *CREAMS: A field scale model for chemicals, runoff, and erosion from agricultural management systems*. U.S. Department of Agriculture, Science and Education Administration.

Lal, R., Ahmadi, M., & Bajracharya, R. M. (2000). Erosional impacts on soil properties and corn yield on Alfisols in central Ohio. *Land Degradation & Development*, *11*(6), 575–585. https://doi.org/10.1002/1099-145X(200011/12)11:6<575::AID-LDR410>3.0.CO;2-N

Leonard, R. E., Knisel, W. G., & Still, D. (1987). GLEAMS: Groundwater Loading Effects of Agricultural Management Systems. *Transactions of the ASABE*, *30*, 1403–1418.

Leopold, L. B. (1951). Rainfall Frequency: An aspect of climatic variation. *Eos, Transactions American Geophysical Union*, *32*(3), 347–357. https://doi.org/10.1029/TR032i003p00347

Lin, C.-Y., Lin, W.-T., & Chou, W.-C. (2002). Soil erosion prediction and sediment yield estimation: the Taiwan experience. *Soil and Tillage Research*, *68*(2), 143–152. https://doi.org/10.1016/S0167-1987(02)00114-9

Liu, C.-Y., Aryastana, P., Liu, G.-R., & Huang, W.-R. (2020). Assessment of satellite precipitation product estimates over Bali Island. *Atmospheric Research, 244*, 105032. https://doi.org/10.1016/j.atmosres.2020.105032

Maeda, E. E., Pellikka, P. K. E., Siljander, M., & Clark, B. J. F. (2010). Potential impacts of agricultural expansion and climate change on soil erosion in the Eastern Arc Mountains of Kenya. *Geomorphology*, *123*(3–4), 279–289. https://doi.org/10.1016/j.geomorph.2010.07.019

Markose, V. J., & Jayappa, K. S. (2016). Soil loss estimation and prioritization of sub-watersheds of Kali River basin, Karnataka, India, using RUSLE and GIS. *Environmental Monitoring and Assessment*, *188*(4), 225. https://doi.org/10.1007/s10661-016-5218-2

Millward, A. A., & Mersey, J. E. (1999). Adapting the RUSLE to model soil erosion potential in a mountainous tropical watershed. *CATENA, 38*(2), 109–129. https://doi.org/10.1016/S0341-8162(99)00067-3

Nahib, I., Wahyudin, Y., Amhar, F., Ambarwulan, W., Nugroho, N. P., Pranoto, B., Cahyana, D., Ramadhani, F., Suwedi, N., Darmawan, M., Turmudi, T., Suryanta, J., & Karolinoerita, V. (2024). Analysis of Factors Influencing Spatial Distribution of Soil Erosion under Diverse Subwatershed Based on Geospatial Perspective: A Case Study at Citarum Watershed, West Java, Indonesia. *Scientifica*, *2024*, 1–20. https://doi.org/10.1155/2024/7251691

Nearing, M. A., Foster, G. R., Lane, L. J., & Finkner, S. C. (1989). A Process-Based Soil Erosion Model for USDA-Water Erosion Prediction Project Technology. *Transactions of the ASAE*, *32*(5), 1587–1593. https://doi.org/10.13031/2013.31195

Neitsch, S. L., Williams, J. R., Arnold, J. G., & Kiniry, J. R. (2011). *Soil and Water Assessment Tool Theoretical Documentation Version 2009*.

Obaid, H. A., & Shahid, S. (2017). Soil erosion susceptibility of Johor River basin. *Water and Environment Journal, 31*(3), 367–374. https://doi.org/10.1111/wej.12252

Okiria, E., Keigo, N., Nishimura, S., & Kobayashi, Y. (2025). TopEros: An Integrated Hydrology and Multi-Process Erosion Model—A Comparison with MUSLE. *Hydrology, 12*(11), 309. https://doi.org/10.3390/hydrology12110309

PERDIRJEN-BPDASPS. (2013). *Peraturan Direktur Jenderal Bina Pengelolaan Daerah Aliran Sungai dan Perhutanan Sosial Nomor P.4/V-SET/2013 tentang Petunjuk Teknis Penyusunan Data Spasial Lahan Kritis*.

Pham, T. G., Degener, J., & Kappas, M. (2018). Integrated universal soil loss equation (USLE) and Geographical Information System (GIS) for soil erosion estimation in A Sap basin: Central Vietnam. *International Soil and Water Conservation Research*, *6*(2), 99–110. https://doi.org/10.1016/j.iswcr.2018.01.001

Renard, K. G. (1997). *Predicting Soil Erosion by Water: A Guide to Conservation Planning with the Revised Universal Soil Loss Equation (RUSLE)*. U.S. Department of Agriculture, Agricultural Research Service.

Romdania, Y., & Herison, A. (2024). The effect of steep slopes on the application of the USLE, RUSLE, and MUSLE methods. *ASEAN Engineering Journal*, *14*(1), 229–236. https://doi.org/10.11113/aej.v14.20567

Ruhe, R. V., & Scholtes, W. H. (1956). Ages and Development of Soil Landscapes in Relation to Climatic and Vegetational Changes in Iowa. *Soil Science Society of America Journal*, *20*(2), 264–273. https://doi.org/10.2136/sssaj1956.03615995002000020029x

Souidi, Z., Hamimed, A., & Donze, F. (2014). Cartographie du risque de dégradation des terres en région semi-aride Cas des Monts de Beni Chougrane dans le Tell occidental algérien. *Geo-Eco-Trop*, *38*(1), 85–102.

Syaf, H., Abadi, M., Ode Hasani, U., Basri, A., Kasno Arief, L., & Gandri, L. (2022). Penilaian Kinerja Pengelolaan DAS Poleang di Sulawesi Tenggara Berdasarkan Indikator Kondisi Lahan. *Jurnal Ilmiah Membangun Desa Dan Pertanian*, *7*(5), 188–199. https://doi.org/10.37149/jimdp.v7i5.132

Tang, J., Cheng, X., Zhu, B., Gao, M., Wang, T., Zhang, X., Zhao, P., & You, X. (2015). Rainfall and tillage impacts on soil erosion of sloping cropland with subtropical monsoon climate — A case study in hilly purple soil area, China. *Journal of Mountain Science*, *12*(1), 134–144. https://doi.org/10.1007/s11629-014-3241-8

Tetford, P. E., Desloges, J. R., & Nakassis, D. (2017). Modelling surface geomorphic processes using the RUSLE and specific stream power in a GIS framework, NE Peloponnese, Greece. *Modeling Earth Systems and Environment*, *3*(4), 1229–1244. https://doi.org/10.1007/s40808-017-0391-z

Thomas, J., Joseph, S., & Thrivikramji, K. P. (2018a). Estimation of soil erosion in a rain shadow river basin in the southern Western Ghats, India using RUSLE and transport limited sediment delivery function. *International Soil and Water Conservation Research*, *6*(2), 111–122. https://doi.org/10.1016/j.iswcr.2017.12.001

Thomas, J., Joseph, S., & Thrivikramji, K. P. (2018b). Assessment of soil erosion in a tropical mountain river basin of the southern Western Ghats, India using RUSLE and GIS. *Geoscience Frontiers, 9*(3), 893-906.https://doi.org/10.1016/j.gsf.2017.05.011

Toubal, A. K., Achite, M., Ouillon, S., & Dehni, A. (2018). Soil erodibility mapping using the RUSLE model to prioritize erosion control in the Wadi Sahouat basin, North-West of Algeria. *Environmental Monitoring and Assessment*, *190*(4), 210. https://doi.org/10.1007/s10661-018-6580-z

Vijith, H., & Dodge-Wan, D. (2018). Spatio-temporal changes in rate of soil loss and erosion vulnerability of selected region in the tropical forests of Borneo during last three decades. *Earth Science Informatics, 11*(2), 171–181. https://doi.org/10.1007/s12145-017-0321-7

Wang, G., Wente, S., Gertner, G. Z., & Anderson, A. (2002). Improvement in mapping vegetation cover factor for the

universal soil loss equation by geostatistical methods with Landsat Thematic Mapper images. *International Journal of Remote Sensing*, *23*(18), 3649–3667. https://doi.org/10.1080/01431160110114538

Wijesundara, N. C., Abeysingha, N. S., & Dissanayake, D. M. S. L. B. (2018). GIS-based soil loss estimation using RUSLE model: a case of Kirindi Oya river basin, Sri Lanka. *Modeling Earth Systems and Environment*, *4*(1), 251–262. https://doi.org/10.1007/s40808-018-0419-z

Williams, J. R. (1975). Sediment routing for agricultural watersheds[1]. *JAWRA Journal of the American Water Resources Association*, *11*(5), 965–974. https://doi.org/10.1111/j.1752-1688.1975.tb01817.x

Williams, J. R., & Berndt, H. D. (1977). Sediment Yield Prediction Based on Watershed Hydrology. *Transactions of the ASAE*, *20*(6), 1100–1104. https://doi.org/10.13031/2013.35710

Williams, J. R., Nicks, A. D., & Arnold, J. G. (1985). Simulator for Water Resources in Rural Basins. *Journal of Hydraulic Engineering*, *111*(6), 970–986. https://doi.org/10.1061/(ASCE)0733-9429(1985)111:6(970)

Wischmeier, W. H., & Smith, D. D. (1965). *Predicting Rainfall-erosion Losses from Cropland East of the Rocky Mountains: Guide for Selection of Practices for Soil and Water Conservation* (Numbers 282–284). Agricultural Research Service, U.S. Department of Agriculture.

Wischmeier, W. H., & Smith, D. D. (1978). *Predicting Rainfall Erosion Losses: A Guide to Conservation Planning*. Department of Agriculture, Science and Education Administration.

Zhang, X.-C. J. (2012). Cropping and Tillage Systems Effects on Soil Erosion under Climate Change in Oklahoma. *Soil Science Society of America Journal*, *76*(5), 1789–1797. https://doi.org/10.2136/sssaj2012.0085

SAŽETAK

Usporedba modela za predviđanje erozije USLE, MUSLE i RUSLE u slijevu rijeke Poleang

Vodna erozija predstavlja ozbiljan globalni problem zbog degradacije zemljišta, a Indonezija je također suočena s tim problemom. Ovaj je fenomen posljednjih desetljeća dodatno pojačan klimatskim promjenama i antropogenim zahvatima u prirodni okoliš. Iako empirijsko modeliranje predstavlja prikladan pristup za predviđanje degradacije tla, njegova primjena na velikim područjima bez mjernih postaja često je ograničena nedostatkom i neujednačenošću podataka. Ovo istraživanje procjenjuje i uspoređuje učinkovitost triju modelskih okvira temeljenih na USLE-u u kvantificiranju erozije uzrokovane vodom u slijevu rijeke Poleang. Dobivene procjene specifične erozije na području slijeva rijeke Poleang iznose 252 t ha^{-1} god^{-1}, 210 t ha^{-1} god^{-1} i 230 t ha^{-1} god^{-1}. Sva tri modela dala su relativno slične procjene uz vrijednosti koeficijenta determinacije (R^2) u rasponu od 91 % do 99 %. Uočeno je da model USLE pokazuje izraženiju prostornu heterogenost raspodjele rizika od erozije u odnosu na modele MUSLE i RUSLE. U tom se kontekstu faktor pokrova vegetacije pokazao kao ključan parametar za objašnjenje povišenih stopa erozije na istraživanome području.

Ključne riječi:
geoprostorna analiza, procjena gubitka tla, GIS-integrirano modeliranje, modeli temeljeni na USLE-u, slijev rijeke Poleang

Author's contribution

Septianto Aldiansyah: conceptualization, data curation, formal analysis, funding acquisition, investigation, methodology, software, writing – original draft and writing – review & editing. **Amniar Ati**: conceptualization, software, visualization, writing – original draft and writing – review & editing. **Fitriyani Saudi**: validation, writing – original draft and writing – review & editing. **Andrias Andrias**: project administration, supervision
All authors have read and agreed to the published version of the manuscript.